Coarsening dynamics / Dynamique de *coarsening*

# Coarsening in fluid phase transitions

## Coarsening *dans les transitions en phase fluide*

Subir K. Das [a,*], Sutapa Roy [a,b,c], Jiarul Midya [a]

[a] *Theoretical Sciences Unit, Jawaharlal Nehru Centre for Advanced Scientific Research, Jakkur P.O., Bangalore 560064, India*
[b] *Max-Planck-Institut für Intelligente Systeme, Heisenbergstraße 3, 70569 Stuttgart, Germany*
[c] *Institut für Theoretische Physik IV, Universität Stuttgart, Pfaffenwaldring 57, 70569 Stuttgart, Germany*

A B S T R A C T

We review the understanding of the kinetics of fluid phase separation in various space dimensions. Morphological differences, percolating or disconnected domains, based on overall composition in a binary liquid or on density in a vapor–liquid system, are discussed. Depending upon the morphology, various possible mechanisms for domain growth are pointed out and discussions of corresponding theoretical predictions are provided. On the computational front, useful models and simulation methodologies are presented. Theoretically predicted growth laws have been tested via molecular dynamics simulations of vapor–liquid transitions. In the case of a disconnected structure, the mechanism has been confirmed directly.

© 2015 Académie des sciences. Published by Elsevier Masson SAS. All rights reserved.

R É S U M É

Nous passons en revue la compréhension de la cinétique de séparation de phases fluides dans diverses dimensions d'espace. Les différences morphologiques, les domaines de percolation ou déconnectés, basés sur la composition totale binaire ou sur la densité dans un système vapeur–liquide, sont discutés. Selon la morphologie, les différents mécanismes possibles sont présentés et les prédictions théoriques correspondantes discutées. Du côté du calcul par ordinateur, des modèles utiles et des méthodes de simulation sont présentées. Des lois de croissance prédites théoriquement ont été testées au moyen de simulations de dynamique moléculaire des transitions vapeur–liquide. Dans le cas d'une structure déconnectée, le mécanisme a été confirmé directement.

© 2015 Académie des sciences. Published by Elsevier Masson SAS. All rights reserved.

## 1. Introduction

Topics related to phase transitions have received significant attention over many decades [1–11]. The evolution of a system from one equilibrium phase to another is a non-equilibrium phenomenon and happens via nucleation [1–6] and growth [5,7–11] of domains. Let us consider a liquid or solid binary mixture $(A + B)$ that exhibits immiscibility (demixing

transition). When such a system is quenched inside the miscibility gap, say via variation of temperature ($T$), from a homogeneously mixed state, it becomes unstable to fluctuations and moves towards the coexisting phase-separated state via the formation and growth of domains rich in $A$ and $B$ particles. For a vapor–liquid transition, the approach to the new equilibrium occurs via the growth of particle-rich and particle-poor regions. The objective of this review is to discuss developments in the understanding of such kinetics [1–49], with a focus on phase-separating fluid systems [20–49].

Typically, the growth of domains is a scaling phenomenon [9], i.e., there exists self-similarity of domain patterns at two different times, despite a change in length scale $\ell(t)$, the average size of domains at time $t$. This is captured in the scaling properties [9]:

$$C(r, t) \equiv \tilde{C}[r/\ell(t)] \tag{1}$$

$$S(k, t) \equiv \ell(t)^d \tilde{S}[k\ell(t)] \tag{2}$$

$$P(\ell_d, t) \equiv \ell(t)^{-1} \tilde{P}[\ell_d/\ell(t)] \tag{3}$$

of the two-point equal time correlation function ($C$), structure factor ($S$) and domain size distribution function ($P$). In Eqs. (1)–(3), $r$ is the distance between two points ($\vec{r}_i$ and $\vec{r}_j$), $k$ is the wave vector, $\ell_d$ is the size of a domain, and $d$ is the system dimensionality. There $\tilde{C}(x)$, $\tilde{S}(y)$ and $\tilde{P}(z)$ are master functions, independent of time. The above-mentioned correlation function is calculated as [9]

$$C(r, t) = <\psi(\vec{r}_i, t)\psi(\vec{r}_j, t)> - <\psi(\vec{r}_i, t)><\psi(\vec{r}_j, t)> \tag{4}$$

where $\psi$ is the relevant order parameter for the transition. $S(k, t)$ is the Fourier transform of $C(r, t)$. The scalar notations $r$ and $k$ imply spherical isotropy and are applicable to systems without any bias such that the structures are isotropic in a statistical sense. The angular brackets in Eq. (4) are for statistical averaging.

Typically, $\ell(t)$ grows with time in power-law fashion as [9]:

$$\ell(t) \sim t^{\alpha} \tag{5}$$

The growth exponent $\alpha$ depends upon $d$, morphology, the number of order parameter components, hydrodynamic effects, and order-parameter conservation [9]. In out-of-equilibrium systems, as is clear from Eq. (4), the order parameter $\psi$ is a function of space and time. In a magnetic system, this can be identified with the local magnetization, in a binary mixture with the local difference between the concentration of the two species, for a vapor–liquid system with the local density. Depending upon the type of transition, the total order-parameter (the local value integrated over the whole system) may or may not remain the same at all times. For instance, in a paramagnetic-to-ferromagnetic transition, where, starting from a zero net magnetization, the system gets spontaneously magnetized, the order parameter is a non-conserved quantity. On the other hand, for all types of phase-separating systems, assuming that there is no chemical conversion or flow of material between the system and a reservoir, this is a conserved quantity. In this paper, we will deal only with conserved scalar order parameter.

The major fraction of the literature in kinetics of phase transitions is related to the behavior of $C(r, t)$ and to the understanding of the exponent $\alpha$. However, there exist other interesting aspects, e.g., aging [50] and the persistence of the local order parameter in its original state [51]. In aging phenomena, typically one studies the two-time quantities, e.g., the order-parameter autocorrelation function [50]

$$C_{\text{age}}(t, t_{\text{w}}) = <\psi(\vec{r}_i, t)\psi(\vec{r}_i, t_{\text{w}})> - <\psi(\vec{r}_i, t)><\psi(\vec{r}_i, t_{\text{w}})> \tag{6}$$

where $t_{\text{w}}$ and $t$ ($> t_{\text{w}}$) are respectively the waiting and observation times. Even though the time translation invariance is not obeyed by $C_{\text{age}}(t, t_{\text{w}})$ in out-of-equilibrium systems, this quantity is expected to exhibit scaling [50] with respect to $t/t_{\text{w}}$. An objective in studies related to aging is to obtain scaling functions for $C_{\text{age}}$ or for other two-time quantities of relevance, in different types of phase transitions.

Each of these aspects are better understood in the non-conserved order parameter case [9]. For the conserved order parameter case, significant progress has been made only with respect to the growth exponent $\alpha$, especially for solid binary mixtures [12–18]. For the latter class of systems, diffusion (via evaporation and condensation) is the only transport mechanism, and the growth is characterized by a single exponent, except for very low temperatures. In fluids, however, no single exponent describes the entire growth process [9]. This is due to the faster transport of material at late times. Manifestation of such fast transport may happen in different ways, depending upon system dimensionality and domain pattern. Thus, kinetics of phase separation in fluids is a richer and challenging area. In spite of that, reasonable progress has been made [20–49]. The aim of the article is to review some of these works in brief.

The rest of the article is organized as follows. In Section 2 we discuss the theoretical progress. Section 3 is devoted to the discussion of models and computational methods. Representative computational results are presented in Section 4. Finally, Section 5 concludes the paper with a brief summary and outlook.
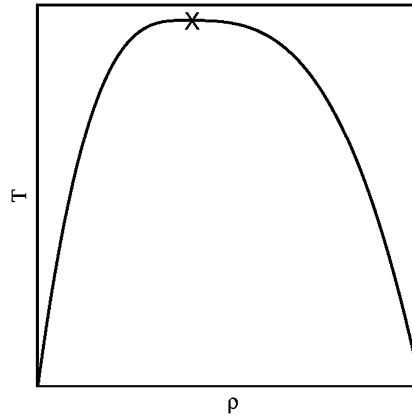
**Fig. 1.** Schematic phase diagram for vapor–liquid coexistence in the $T$-vs-$\rho$ plane. The critical point is marked by a cross. The left and right branches represent respectively the vapor and the liquid densities.
From Molecular Simulation **41** (2015) 382.

## 2. Theories

In a solid binary mixture, the rate of change of domain size is associated with the chemical potential gradient as [13] $d\ell/dt \sim |\vec{\nabla}\mu|$. Using the dimensionality of $\mu$ as $\gamma/\ell$, $\gamma$ being the (domain) interfacial tension, and assuming that a gradient exists over the length of the domain size, one obtains [13]

$$\frac{d\ell}{dt} \sim \frac{\gamma}{\ell^2} \tag{7}$$

The solution to Eq. (7) provides $\alpha = 1/3$, referred to as the Lifshitz–Slyozov (LS) law [12], and is understood to be valid for any domain growth occurring via simple diffusive mechanism.

The early stage of fluid phase separation is also dominated by diffusion, with an expected $\alpha$ value of 1/3. At late times, hydrodynamic effects become more important. As already mentioned, while for phase separation in solid mixtures system dimensionality and domain morphology do not play important roles [18], they become crucial for the selection of the mechanism in fluids. In some cases, different mechanisms may give rise to a same value of the growth exponent. Thus, very direct computational or experimental probes are necessary to validate a particular one. We will discuss below some relevant mechanisms briefly.

Typically, phase separating systems exhibit interconnected or droplet morphology, depending upon the overall composition or density of the system. In Fig. 1, we show a vapor–liquid coexistence curve in the temperature-versus-density ($\rho$) plane. There the left branch corresponds to the vapor-phase density and the right one to the liquid-phase density. For a binary mixture phase separation, the appropriate abscissa variable is the concentration of one of the species. For a density or a composition very close to the coexistence curve (vapor branch in vapor–liquid transitions), a droplet-like pattern is visible, from the very beginning. In this under-saturation case, the system requires fluctuations involving large length scales to nucleate stable droplets that can grow. Such events, depending upon the proximity of the coexistence curve, may be rare and the phase separation can be delayed. On the other hand, far from the coexistence curve, the system falls unstable to infinitesimal fluctuations and the corresponding phase separation process is referred to as the spinodal decomposition. Typically, in this case, the domain morphology is percolating. Here we caution the reader that at late time droplet structures can emerge from the percolating morphology as well [36], if the system is even slightly away from the critical composition or density. This is decided by the percolation threshold. In $d = 2$, for instance, the threshold composition for a symmetric binary mixture is $50 : 50$, i.e., the critical one. While during the time evolution of a solid binary mixture, with marginally off-critical composition, this phenomenon may not be observable, in fluids this is observable within the computationally accessible time-scales of the simulations of coarse-grained models [36].

Let us first consider the case of a percolating domain morphology for which interesting hydrodynamic mechanisms have been proposed. Because of experimental realizability, we will first take up the $d = 3$ case. The hydrodynamic regime is divided into two subregimes [9], viz., viscous and inertial. These we discuss below, following Siggia [22] and Furukawa [23,24], using the Navier–Stokes (NS) equation:

$$\rho \frac{D}{Dt}\vec{v} - \rho \nu \nabla^2 \vec{v} = -\vec{\nabla}p \tag{8}$$

In Eq. (8), $\rho$ is the mass density, $\vec{v}$ is the fluid velocity, $\nu$ is the kinematic viscosity, $p$ is the pressure and $D/Dt = d/dt + (\vec{v}\cdot\vec{\nabla})$. In $D\vec{v}/Dt$, both terms stand for acceleration, as can be checked dimensionally. The second one is related to convection, where the acceleration is generated by the space-dependent velocity. Eq. (8) is essentially related to the balance of the force coming from pressure with that due to frictions. In an incompressible fluid ($\vec{\nabla} \cdot \vec{v} = 0$), in the absence of

any external influence like gravity, the relevant term on the right-hand side comes from the gradient in the free energy, being given by $\gamma/\ell^2$. On the left-hand side, the first term can be treated as inertial friction and the second one is related to dissipative friction originating from viscous drag. Via dimensional substitutions, $Dv/Dt \equiv v/t$ and $\nabla^2 v \equiv -v/\ell^2$; one writes, after multiplying both sides of Eq. (8) by $vt$,

$$\rho v^2 + \frac{\rho v}{\ell} v = \frac{\gamma}{\ell} \tag{9}$$

The second term on the left-hand side of Eq. (9) is related to the inverse of the time-dependent Reynolds number and is important at earlier part of the hydrodynamic regime, providing viscous growth. At a later time, when $\ell$ becomes large, the first term dominates, giving rise to the inertial hydrodynamic growth. Thus, in the first part of hydrodynamic growth, it is equivalent to equating the interfacial free-energy density with the viscous stress and in the second part, the same with the kinetic energy density [22]. With the understanding that there exist unique time and length scales in the problem, one identifies $v$ with $d\ell/dt$. Then, in the viscous regime, one obtains

$$\frac{d\ell}{dt} = \frac{\gamma}{\rho v} \tag{10}$$

and in the inertial regime

$$\frac{d\ell}{dt} = \sqrt{\frac{\gamma}{\rho \ell}} \tag{11}$$

The solutions to Eqs. (10) and (11) provide $\alpha = 1$ and $2/3$, respectively.

Recall that our discussion is related to an interconnected domain morphology, having a tube-like structure for $d = 3$. The fast advective transport of material through these undulating tubes happens due to a driving force calculable from the interfacial tension and the domain size. In $d = 2$, the analogue of a tube is a strip. San Miguel et al. [25] argued that fluctuations along the linear boundaries of these strips significantly increase the interfacial free energy due to the increase in the curvature. This mechanism thus lacks instability. According to these authors, unlike for $d = 3$, where a crossover from $\alpha = 1/3$ to 1 occurs, the 2-d fluid may encounter a crossover from $1/3$ to $1/2$, the latter coming from an interface diffusion mechanism [25]. There a crossover from $\alpha = 1/3$ to 1 will require large fluctuations, and may become possible only at very high temperatures.

Note that, in case of droplet morphology, the growth description cannot be provided via NS equation [9]. As opposed to solid binary mixtures, droplets in fluids are significantly mobile. This gives rise to, in addition to the standard evaporation–condensation like process, another growth mechanism involving random diffusion and collision of droplets, proposed by Binder and Stauffer (BS) [20–22]. These are inelastic collisions, following which the colliding partners merge, forming a bigger droplet and reducing the droplet density ($n$). For the decay of $n$, one can write [22]

$$\frac{dn}{dt} = -K D_\ell \ell n^2 \tag{12}$$

where $K$ is a constant and $D_\ell$ is the diffusion constant for a droplet of size $\ell$. For a discussion on the value of $K$ (an error exists in Ref. [11]), see Refs. [22,26–28]. Following the Stokes–Einstein–Sutherland relation [52], $D_\ell \ell$ can be treated as a constant. Using $n \sim 1/\ell^d$, one obtains [22]

$$\frac{d\ell}{dt} \propto \frac{1}{\ell^{d-1}} \tag{13}$$

The solution to Eq. (13) provides $\alpha = 1/d$. Thus, for $d = 2$, the BS value of $\alpha$ is the same as that for the interface diffusion mechanism of San Miguel et al. On the other hand, for $d = 3$, the BS mechanism provides a value of $\alpha$ that coincides with the LS value. It is expected that the amplitudes will be different for different mechanisms that provide the same exponents. For instance, for $d = 3$, LS mechanism should have a smaller amplitude than that of the BS mechanism [26–28]. Direct verification of the latter is possible via computer simulations [45]. Tanaka [26–28] argued that in a high droplet density situation, the motion of the droplets will not be random, due to inter-droplet interaction. However, the incorporation of such fact merely changes the growth amplitude. The presence of such interaction can be verified by calculating the mean-squared displacements (MSD) [52] of the droplets.

The pictures presented above are primarily meant for the kinetics of incompressible liquid–liquid phase separation. Nevertheless, they may apply for vapor–liquid phase separation to a good extent. This, however, requires verification.

## 3. Models and methods

The kinetics of phase separation in solid binary mixtures at an atomistic level have been traditionally studied via Monte Carlo (MC) simulations [53] of the nearest-neighbor Ising model

$$H = -J \sum_{<ij>} S_i S_j; \quad J > 0; \ S_i = \pm 1 \tag{14}$$

on a regular lattice. Here, an up spin ($S_i = +1$) corresponds to an $A$ particle and a down spin ($S_i = -1$) to a $B$ particle. In this model, the kinetics is introduced via the Kawasaki exchange [53] trial moves, in which the positions of two nearest-neighbor particles are interchanged. These MC moves are accepted according to the standard Metropolis algorithm [53]. At the coarse-grained level, one solves the Cahn–Hilliard (CH) equation [9]

$$\frac{\partial \psi(\vec{r}, t)}{\partial t} = -\nabla^2 \Big[ \psi(\vec{r}, t) + \nabla^2 \psi(\vec{r}, t) - \psi^3(\vec{r}, t) \Big] \tag{15}$$

where the order parameter $\psi$ can be thought of as being obtained from the coarse-graining of the Ising spins over a length scale of the order of the equilibrium correlation length $\xi$. Thus, the CH equation provides the advantage of exploring large effective length scale within a practically accessible computation time. Eq. (15) can be obtained from the Ising model via a master equation approach with Kawasaki kinetics as an input [54,55]. Despite the latter being a direct and rigorous approach, in this article we will present a phenomenological derivation. This equation is solved on a regular lattice, typically via an Euler discretization technique [55].

According to the nomenclature of Hohenberg and Halperin [56], the above model is referred to as model B. In fluids, at coarse-grained level the kinetics is typically studied via model H [56], which is a combination of model B and of the NS equation, the latter taking care of the fluid flow. To describe this model, the derivation of the CH equation [9] will be of help. Recalling that we are dealing with a conserved order parameter, one writes the continuity equation

$$\frac{\partial \psi}{\partial t} = -\vec{\nabla} \cdot \vec{J}_c \tag{16}$$

where the current $\vec{J}_c$ comes from the gradient of the chemical potential $-\vec{\nabla}\mu$, setting the appropriate transport coefficient (concentration conductivity for a binary fluid) to unity. Eq. (15) can be arrived at by knowing that the chemical potential can be obtained from the functional derivative as

$$\mu = \frac{\delta F[\psi(\vec{r}, t)]}{\delta \psi(\vec{r}, t)} \tag{17}$$

the free energy functional being the Ginzburg–Landau one

$$F = k_B T \int d\vec{r} [-a\psi^2 + b\psi^4 + c(\vec{\nabla}\psi)^2] \tag{18}$$

where the positive coefficients $a$, $b$, and $c$ are temperature dependent. Often these coefficients are scaled in such a way that the final form is parameter free, as in Eq. (15).

The model H equations read [9], in the incompressible limit, as:

$$\frac{\partial \psi}{\partial t} + \vec{v} \cdot \vec{\nabla}\psi = \nabla^2 \mu \tag{19}$$

$$\rho \frac{D\vec{v}}{Dt} - \nu\nabla^2\vec{v} = -\vec{\nabla}p - \psi\vec{\nabla}\mu \tag{20}$$

In this limit, the pressure term on the right-hand side of Eq. (20) can be eliminated via the condition $\vec{\nabla} \cdot \vec{v} = 0$. The drive will come essentially from the second term on the right-hand side, as discussed before, in the context of Eq. (8). In addition to the pure CH and NS equations, there are thus additional terms in Eqs. (19) and (20), coming from the coupling between the velocity and the order-parameter fields. This is justifiable, e.g., by the fact that the current $\vec{J}_c$ in the CH equation is expected to be influenced by the velocity field, providing a term proportional to $\psi\vec{v}$ and that the chemical potential gradient should provide a driving force to affect the velocity field in the NS equation. Again, these equations can be solved on a regular lattice.

Even though the construction of this model is very much justifiable phenomenologically, a microscopic derivation like the CH equation [54] is still lacking. Such an objective can possibly be achieved [57] via the construction of free-energy functionals by taking density and velocity distributions as inputs from molecular dynamics (MD) simulations at various coarse-grained levels, by appropriately adjusting the effective inter-particle potential at successive steps. The success of a multi-scale method like this may seem obvious, but has never been demonstrated. If it works for the present problem, the method will prove useful in justifying similar (elegant) phenomenological models in more complex problems, like with active matter [58].

The incorporation of the coupled terms in Eqs. (19) and (20), in a sense, guarantees the simultaneous growth in the velocity and density fields. While such facts have been reported from lattice Boltzmann simulations [10,34], they are lacking in MD simulations, even though the latter is more direct and accurate. Thus, a microscopic justification of the model and, possibly via the similar multiscale method, an understanding of the importance of additional (higher-order) terms, is needed.

As can be guessed from the above discussion, at atomistic level, the kinetics of fluid phase separation is studied via MD simulations [59–61] in which hydrodynamics can be easily implemented. For this purpose, the interatomic interactions are popularly incorporated via the well-known Lennard-Jones (LJ) potential

$$u(r) = 4\varepsilon\left[\left(\frac{\sigma}{r}\right)^{12} - \left(\frac{\sigma}{r}\right)^{6}\right] \tag{21}$$

where $r$ $(= |\vec{r}_i - \vec{r}_j|)$ is the distance between two particles at $\vec{r}_i$ and $\vec{r}_j$, $\varepsilon$ is the interaction strength and $\sigma$ is the interparticle diameter. In a binary (or multicomponent) mixture, $\varepsilon$ and $\sigma$ can be chosen to be different for different combinations of species.

In standard MD simulations, the equations of motion are solved in discrete time, typically via Verlet's velocity algorithm [59,60]. The conservation laws of hydrodynamics are perfectly satisfied in a microcanonical ensemble that allows various fluid transport properties to be calculated at the equilibrium. However, concerning the kinetics of phase separation, following a temperature quench, in the course of the system's evolution, the potential energy decreases for energy-driven phase transitions. In a constant energy ensemble, thus, kinetic energy, i.e., temperature increases, destroying the objective of the study. Therefore, simulations in a canonical ensemble, with an appropriate hydrodynamics preserving thermostat, become essential. There are a number of good methods for this purpose, e.g., dissipative particle dynamics [62–64], multiparticle collision dynamics [65], Lowe–Andersen thermostat [66], Nosé–Hoover thermostat [60], etc. In this article, the presented results were obtained via the application of the Nosé–Hoover thermostat (NHT), which will be introduced soon.

## 4. Simulation results

Binary fluid phase separation has been studied via lattice Boltzmann simulations or through simpler solutions to model H equations [34–36] for quenches with critical composition. Though MD simulations in this context are relatively rare, the theoretical expectations for critical quenches are confirmed to a good degree [11,37–41]. Here we focus on vapor–liquid phase separation, for which MD simulations are mostly recent [42–49]. Particular emphasis is placed on off-critical (overall density close to the vapor branch of the coexistence curve) quenches that provide the droplet morphology. The objective is to check to what extent the kinetics of vapor–liquid phase separation is similar to that of an incompressible binary liquid. In this context, we must mention that in dynamic critical phenomena [8,56,67–74] liquid–liquid and vapor–liquid transitions belong to the same universality class. It is important to verify, thus, whether the non-equilibrium dynamics are similar in the two cases. In dynamic critical phenomena, the interest lies in understanding the singularities of various collective transport properties, e.g., viscosities and diffusivities, in the vicinity of the critical or second-order phase transitions.

All results were obtained via a modified LJ model where particles interact as [59]:

$$U(r < r_c) = u(r) - u(r_c) - (r - r_c)\frac{\mathrm{d}u(r)}{\mathrm{d}r}\Big|_{r=r_c}$$

$$U(r \geq r_c) = 0 \tag{22}$$

The cut-off radius $r_c$ $(= 2.5\sigma)$ in Eq. (22) is introduced for faster computation. Note that, in critical phenomena [1,2], LJ potential being a short-range one, this truncation does not alter the universality class. Due to the cut-off of the potential, despite shifting to 0 at $r = r_c$, a discontinuity in the force is created. This may cause a non-smooth behavior in energy (as a function of time) and can possibly be problematic for energy and momentum conservations at the local scale, necessary for the preservation of hydrodynamics. This problem is corrected by incorporating the last term in the first part of Eq. (22).

The phase diagram, the primary requirement before studying the kinetics of phase separation, for atomistic models, can be obtained using both MC and MD simulations. As is well known, equilibrium phase behavior and thermodynamic properties are insensitive to the ensemble and technicality related to transport mechanism. Thus, MC simulations with "smart" ensembles are advantageous for this purpose, compared to MD. For vapor–liquid phase transitions, popular choices are grandcanonical and "Gibbs" ensemble MC methods [53,60,75]. In a grandcanonical ensemble, alongside the particle displacement moves, one allows density to fluctuate inside the simulation box, by deleting or adding particles. To incorporate these additional moves, one needs to introduce the chemical potential in the Boltzmann factor while performing the MC simulations. On the other hand, in the Gibbs ensemble method one works with two boxes, allowing the particles to move from one box to the other by keeping the total number of particles fixed. In addition, there exist moves related to change in box volumes (by keeping the total volume fixed) and standard particle displacements. Thus, the particle densities in the two boxes fluctuate around different values and their averages correspond to the coexisting vapor and liquid densities on the coexistence curve, when simulations are performed below the critical temperature.

As mentioned, an NHT was applied to study dynamics via MD. There one solves the deterministic equations of motion [60]

$$m\dot{\vec{r}}_i = \vec{p}_i \tag{23}$$

$$\dot{\vec{p}}_i = -\frac{\delta U}{\delta \vec{r}_i} - \Xi\vec{p}_i \tag{24}$$

$$\dot{\Xi} = \frac{\left[\sum\limits_{i=1}^{N}(p_i^2/m) - 3Nk_\mathrm{B}T\right]}{Q} \tag{25}$$

In Eqs. (23)–(25), $m$ is the particle mass (set equal for all), $\Xi$ is a time-dependent drag that adjusts its value depending upon the drift of temperature from the assigned value, $N$ is the number of particles, $k_B$ is the Boltzmann constant, and $Q$ is the coupling strength between the system and the thermostat. From the form of Eq. (25) and the discussion above, it is understood that the instantaneous temperature of the system fluctuates around the assigned temperature $T$. In the NHT scheme, one essentially works with a microcanonical ensemble with a modified Hamiltonian. The results thus obtained are equivalent to those from the canonical ensemble with the original Hamiltonian [60,63].

There exist better hydrodynamics preserving thermostats. But for the present purpose, the NHT appears adequate. The results obtained using this thermostat have been tested against other methods. For example, for $d = 2$, we have compared [49] them with the Lowe–Andersen thermostat (LAT). The LAT is an improvement over the basic Andersen thermostat (AT). In the AT, randomly chosen particles are assigned new velocities (with an overall Maxwell distribution) to keep the temperature at a desired value and thus stochastic in nature, like MC methods. In the LAT, while assigning new velocities, the conservation of local momentum is appropriately taken care of. Further, inside the coexistence region, transport properties of droplets (for equilibrium configurations), calculated via NHT, are found to be in good agreement with the calculations using microcanonical ensemble [46,47]. Also, in a binary fluid, critical behavior of shear viscosity was nicely reproduced via NHT [67]. In addition, from the experience, we feel that the NHT provides a superior control over temperature (which is an important criterion), compared to a few other better hydrodynamics preserving thermostats, particularly in out-of-equilibrium situations.

We will present results [45–47,49] for both $d = 2$ and 3, from MD simulations in periodic square or cubic boxes of linear dimension $L$ (in units of $\sigma$). All results were obtained after averaging over adequately large numbers of independent initial configurations. In the solutions to the equations of motion, we have used time discretization $\Delta t = 0.005\,t_0$, $t_0$ [$= (m\sigma^2/\varepsilon)^{1/2}$] being an LJ time unit. Note that the critical temperature and the critical number density for this model for $d = 3$ respectively are $\simeq 0.9\,\varepsilon/k_B$ and $\simeq 0.3\,\sigma^{-3}$. All results for $d = 3$ correspond to quenches from $T = \infty$ to $0.6\,\varepsilon/k_B$. As expected, the value of $T_c$ for $d = 2$ is lower ($\simeq 0.4\,\varepsilon/k_B$). The quench temperature in this case is $0.25\,\varepsilon/k_B$. For this dimension, we will present results only for the number density $0.02\,\sigma^{-2}$. In the rest of the article, we set $m$, $\sigma$, $\varepsilon$ and $k_B$ to unity.

In Fig. 2a, we present snapshots for $d = 3$ (unless otherwise mentioned, the results are from this dimension) for different overall densities. In Fig. 2b we show the phase diagram of the model in a temperature–density plane, obtained from the Gibbs ensemble simulations. The state points for which the snapshots in Fig. 2a are presented are marked on this phase diagram by crosses. It is clearly seen that as one approaches the vapor branch of the coexistence curve, the morphology becomes more droplet like. Given that we have access to both percolating and droplet structures, a wide variety of mechanisms can be checked.

In Fig. 3, we show a scaling plot of the correlation functions for an overall density that provides droplet morphology, using data from different times. For this calculation, the order parameter $\psi$ at a point is given a value $+1$ if the density there is higher than the overall density $\rho$, and $-1$ otherwise. A nice collapse of data, when plotted versus $r/\ell(t)$, confirms the self-similarity of the structures. Note here that we have obtained $\ell(t)$ from different methods, from the lengths at which $C(r, t)$ decays to a particular value, from the first moment of $P(\ell_d, t)$, as well as by identifying domain boundaries and directly counting the number of particles inside them. For the last method, cube (square for $d = 2$) root of the average number of particles inside the liquid droplets will provide $\ell(t)$. For the sake of brevity, we present results only from the correlation functions.

In Fig. 4, we show plots of $\ell(t)$ vs $t$, for various overall values of $\rho$. It appears that closer to the critical density there is a linear growth, after a brief slow regime, before hitting the finite-size effects. The slower part at the very beginning can be attributed to the LS behavior [12] and the linear one to the hydrodynamic behavior [22–24]. Due to the demanding nature of MD simulations, to the best of our knowledge, a crossover from a linear to $t^{2/3}$ behavior is not yet appropriately observed using this method. However, for intermediate densities, we observed a $t^{2/3}$ behavior even before a linear growth appears. This has been checked [47] via an appropriate finite-size scaling analysis [76], which we do not present here. A possible reason for observing the exponent 2/3 during the early period of the hydrodynamic growth can be the following. In an intermediate density regime, where the interconnectedness of the domain morphology is not very robust, the break-up becomes easier. Due to the competition between growth and break-up, the evolution may become slower than linear, leading to an observation of the exponent 2/3 early enough. For densities very close to the coexistence vapor density, certainly the growth is much slower. We will discuss this in details below [45–47].

In Fig. 5 we take a look at the length scale results for $\rho = 0.05$ on a double-log scale. The flat behavior of the data at the beginning is due to delayed nucleation. A very fast rise after this signals the onset of nucleation (the consistency of the data with the exponent 2/3 in this regime should not be taken seriously), following which the data are consistent with a $t^{1/3}$ growth. As mentioned already, for $d = 3$ this behavior can be due to a LS [12,13] as well as to a BS [20–22] mechanism. To identify the correct mechanism from the multiple possibilities, we do the following exercises.

In Fig. 6, we show plots of $dn/dt$ versus $n$, for two different low values of $\rho$, both providing droplet structure, on a double-log scale. The technical details of the counting of droplets (by identifying them) can be found elsewhere [45–47]. Linear look in both cases confirms a power-law behavior. The solid lines there are proportional to $n^2$, which are consistent with the simulation data. This verifies the starting equation—see Eq. (12)—for deriving the BS [20–22] growth law. We have also checked that between two collisions, the sizes of the droplets remain the same, within minor fluctuations. On the other hand, for LS mechanism it has been observed that the droplets are essentially static. This was studied via application of AT
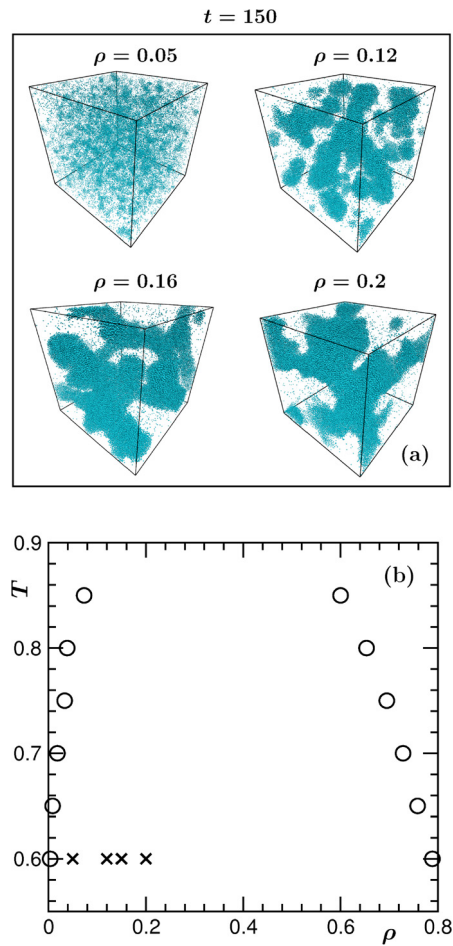
**Fig. 2.** (Color online.) (a) Evolution snapshots for various overall densities $\rho$, obtained from molecular dynamics simulations of the single-component Lennard-Jones model for $d = 3$. In all the cases the time, temperature and the system size were fixed to $t = 150$, $T = 0.6$ and $L = 80$. (b) A phase diagram, obtained from Gibbs ensemble simulation, for a $d = 3$ LJ fluid is presented in the temperature-vs.-density plane. The state points for which the snapshots in (a) are presented have been marked with crosses.
Part (a) reproduced with permission from J. Chem. Phys. **139**, 044911 (2013).
© 2013 AIP Publishing LLC
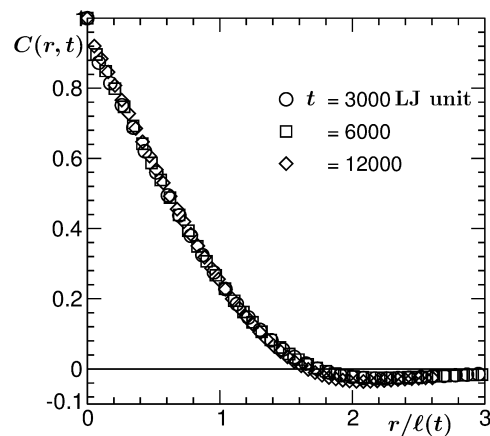


**Fig. 3.** Scaling plot of $C(r,t)$ as a function of $r/\ell(t)$, for $\rho = 0.05$, for $d = 3$. Data from few different times are included. The results correspond to droplet morphology.
From Soft Matter **9** (2013) 4178.
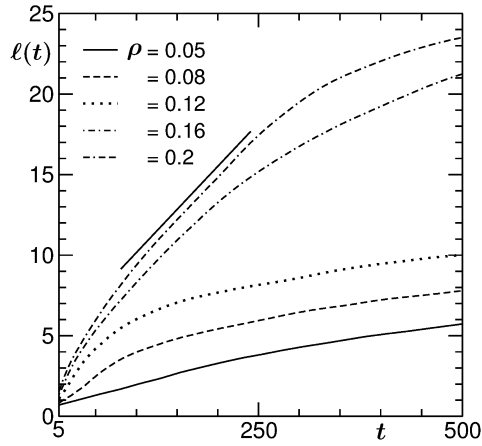
**Fig. 4.** Plots of $\ell(t)$ versus $t$, for different overall values of $\rho$, for $d = 3$. The continuous straight line corresponds to viscous hydrodynamic growth. Reproduced with permission from J. Chem. Phys. **139** (2013) 044911.
© 2013 AIP Publishing LLC
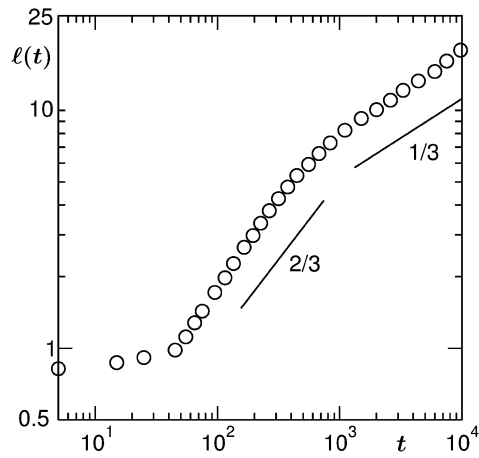


**Fig. 5.** Log–log plot of $\ell$ versus $t$, for $d = 3$, for $\rho = 0.05$. This corresponds to droplet morphology. The solid lines stand for power laws, the exponents being mentioned in the figure.
From Phys. Rev. E **85** (2012) 050602(R).
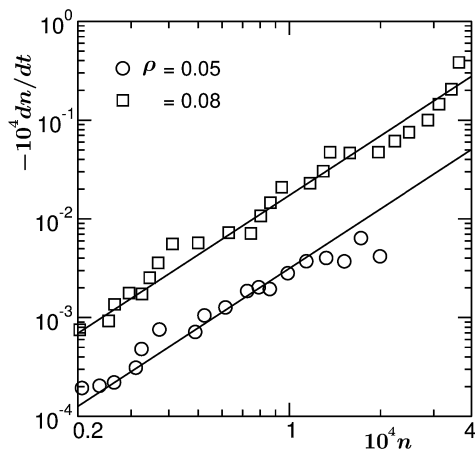


**Fig. 6.** Plots of $dn/dt$ versus $n$, $n$ being the droplet density. Results for two values of $\rho$, for $d = 3$, are included. The solid lines are proportional to $n^2$. For $\rho = 0.08$ a multiplicative factor 5 was used to separate the data sets from each other.
Reproduced with permission from J. Chem. Phys. **139** (2013) 044911.
© 2013 AIP Publishing LLC
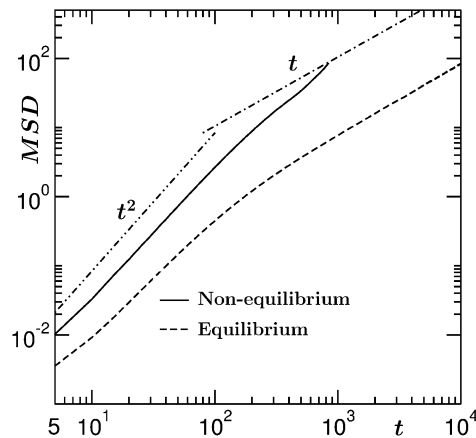
**Fig. 7.** Mean squared displacements for droplets in equilibrium and non-equilibrium situations are plotted versus time. The droplets are of similar sizes. The quadratic and linear behaviors, corresponding to ballistic and diffusive regimes, are appropriately marked by different lines. The results are for $d = 3$. From Soft Matter **9** (2013) 4178.
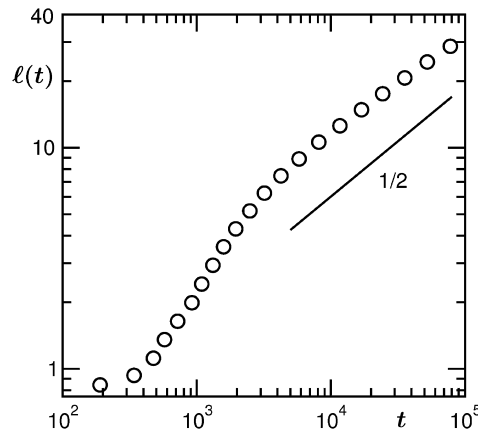


**Fig. 8.** Plot of $\ell$ vs $t$, obtained from the simulations of LJ fluid for $d = 2$. The solid line has a $t^{1/2}$ behavior. The results correspond to a droplet morphology for an overall density $\rho = 0.02$.

that provides purely diffusive growth. The combination of these tests rule out the importance of the LS mechanism in the present context.

Next, we come to the point of inter-droplet interaction. To understand it, we have calculated the MSD [52] of individual droplets [45,46] as

$$\text{MSD} = < (\vec{R}_{CM}(t) - \vec{R}_{CM}(0))^2 > \tag{26}$$

where $\vec{R}_{CM}(t)$ is the location of the center of mass of the droplet under consideration at time $t$. In Fig. 7, we show MSD values for a typical droplet during non-equilibrium evolution (see the continuous line), as a function of time. Note that the duration over which such data can be presented is dictated by the average collision interval. This is larger for low droplet density and increases with the evolution of the system. In the same graph, we showed a corresponding plot for a droplet in equilibrium situation, of approximately the same size as in the non-equilibrium case. The difference between the two cases is significant. As can be seen, on a double-log scale, at a late time, the equilibrium droplet exhibits a linear behavior, confirming a Brownian motion. The super-linear behavior in the non-equilibrium case can be due to inter-droplet interactions, as stated by Tanaka [26–28].

Finally, in Fig. 8 we show an $\ell$-versus-$t$ plot for $d = 2$ with off-critical composition [49]. Here an exponent $\alpha = 1/2$ is visible, corresponding to the BS mechanism. From the calculation of $dn/dt$, in this dimension also we have confirmed the validity of Eq. (12). For the sake of brevity, we do not present them here. For a higher overall density, an exponent $1/2$, possibly due to the interface diffusion mechanism, was previously observed in this dimension [48], even before the appearance of a linear growth. However, the latter study is very preliminary and since then a number of important developments have happened in the field of computer simulation, in terms of improved methods as well as with respect to the enhancement of computer speed and memory. Thus, these problems can be revisited for superior understanding.

## 5. Conclusion

We have provided a brief review on the kinetics of fluid phase separation. A general discussion on various theoretical pictures, based on system dimensionality and domain morphology, is provided. Methodologies related to coarse-grained and atomistic models are discussed. Particular emphasis was on the simulation methods of molecular dynamics.

Molecular dynamics results for vapor–liquid transitions are presented [45–47,49] for $d = 2$ and 3. These include percolating as well as droplet structures. From these simulations, the domain growths are observed to be consistent with theoretical predictions, despite the fact that most of these predictions are related to phase separation in binary fluids. For the sake of brevity, we have avoided presenting the simulation results on binary fluid mixtures.

Recently, important results and the corresponding understanding have been obtained with respect to aging in fluid phase separation, for binary fluids as well as for vapor–liquid systems, via molecular dynamics simulations [77,78]. In addition, the effects of disorder in the kinetics of fluid phase separation have been looked at [41] and compared with the case of disordered Ising systems. The lack of space, however, prevents us from including these results.

Further, there have been significant activities in the area of kinetics in confined geometry [79–89]. A good number of reports in this context exist in fluid phase separation [83–86,88,89] as well. However, the understanding of these results is not as complete as for pure two- and three-dimensional systems.

Even though there exist significant agreement of the theories with simulations of simple models and experiments, occasionally discrepancies have been reported. In the analysis of simulation as well as experimental results, one needs to choose the right morphologies in the appropriate time regimes. In experiments, care should be taken to remove the external effects, e.g., gravity and impurity. On the other hand, it is possible to do simulation studies of more realistic models [41,90] by incorporating the above-mentioned effects, particularly when improved computational resources are available.

## Acknowledgements

## References

[1] M.E. Fisher, Theory of equilibrium critical phenomena, Rep. Prog. Phys. 30 (1967) 615–730.
[2] H.E. Stanley, Introduction to Phase Transitions and Critical Phenomena, Oxford University Press, 1971.
[3] R. Evans, The nature of the liquid–vapor interface and other topics in the statistical mechanics of non-uniform, classical fluids, Adv. Phys. 28 (1979) 143–200.
[4] K. Binder, Theory of first order phase transitions, Rep. Prog. Phys. 50 (1987) 783–859.
[5] K. Binder, Spinodal decomposition, in: R.W. Cahn, P. Haasen, E.J. Kramer (Eds.), Phase Transformation of Material, in: Materials Science and Technology, vol. 5, VCH, Weinheim, 1991, pp. 405–471.
[6] D. Kashchiev, Nucleation: Basic Theory with Applications, Butterworth–Heinemann, Oxford, 2000.
[7] R.A.L. Jones, Soft Condensed Matter, Oxford University Press, 2002.
[8] A. Onuki, Phase Transition Dynamics, Cambridge University Press, 2002.
[9] A.J. Bray, Theory of phase ordering kinetics, Adv. Phys. 51 (2002) 481–587.
[10] S. Puri, V. Wadhawan (Eds.), Kinetics of Phase Transitions, CRC Press, Boca Raton, 2009.
[11] S.K. Das, Atomistic simulations of liquid–liquid coexistence in confinement: comparison of thermodynamics and kinetics with bulk, Mol. Simul. 41 (2015) 382–401.
[12] I.M. Lifshitz, V.V. Sloyozov, The kinetics of precipitation from supersaturation solid solutions, J. Phys. Chem. Solids 19 (1961) 35–50.
[13] D.A. Huse, Correlation to late-stage behavior in spinodal decomposition: Lifshitz–Slyozov scaling and Monte Carlo simulations, Phys. Rev. B 34 (1986) 7845–7850.
[14] J.F. Marko, G.T. Barkema, Phase ordering in the Ising model with conserved spin, Phys. Rev. E 52 (1995) 2522–2534.
[15] D.W. Heermann, L. Yixue, K. Binder, Scaling solution and finite-size effects in the Lifshitz–Slyozov theory, Physica A 230 (1996) 132–148.
[16] J. Vinals, D. Jasnow, Finite-size-scaling analysis of domain growth in the kinetic Ising model with conserved and nonconserved order parameters, Phys. Rev. B 37 (1998) 9582–9589.
[17] S. Majumder, S.K. Das, Domain coarsening in two dimensions: conserved dynamics and finite-size scaling, Phys. Rev. E 81 (2010) 050102.
[18] S. Majumder, S.K. Das, Temperature and composition dependence of kinetics of phase separation in solid binary mixtures, Phys. Chem. Chem. Phys. 15 (2013) 13209.
[19] T. Blanchard, F. Corberi, L.F. Cugliandolo, M. Pico, How soon after a zero-temperature quench is the fate of the Ising model sealed?, Europhys. Lett. 106 (2014) 66001.
[20] K. Binder, D. Stauffer, Theory for the slowing down of the relaxation and spinodal decomposition of binary mixtures, Phys. Rev. Lett. 33 (1974) 1006–1009.
[21] K. Binder, Theory for the dynamics of "clusters." II. Critical diffusion in binary systems and the kinetics of phase separation, Phys. Rev. B 15 (1977) 4425–4447.
[22] E.D. Siggia, Late stages of spinodal decomposition in binary mixtures, Phys. Rev. A 20 (1979) 595–605.
[23] H. Furukawa, Effect of inertia on droplet growth in a fluid, Phys. Rev. A 31 (1985) 1103–1108.
[24] H. Furukawa, Turbulent growth of percolated droplets in phase separating fluids, Phys. Rev. A 36 (1987) 2288–2292.
[25] M. San Miguel, M. Grant, J.D. Gunton, Phase separation in two-dimensional binary fluids, Phys. Rev. A 31 (1985) 1001–1005.
[26] H. Tanaka, A new coarsening mechanism of droplet spinodal decomposition, J. Chem. Phys. 103 (1995) 2361.
[27] H. Tanaka, Coarsening mechanisms of droplet spinodal decomposition in binary fluid mixtures, J. Chem. Phys. 105 (1996) 10099–10114.
[28] H. Tanaka, New mechanisms of droplet coarsening in phase-separating fluid mixtures, J. Chem. Phys. 107 (1997) 3734–3737.
[29] F. Perrot, P. Guenoun, T. Baumberger, D. Beysens, Y. Garrabos, B. Le Neindre, Nucleation and growth of tightly packed droplets in fluids, Phys. Rev. Lett. 73 (1994) 688–691.

[30] J.P. Delville, C. Lalaude, S. Buil, A. Ducasse, Late stage kinetics of a phase separation induced by a cw laser wave in binary liquid mixtures, Phys. Rev. E 59 (2006) 5804–5818.

[31] J. Hobley, S. Kajimoto, A. Takamizawa, H. Fukumura, Experimentally determined growth exponents during the late stage of spinodal demixing in binary liquid mixtures, Phys. Rev. E 73 (2006) 011502.

[32] D. Beysens, Y. Garrabos, D. Chatain, P. Evesque, Phase transition under forced vibrations in critical $CO_2$, Europhys. Lett. 86 (2009) 16003.

[33] S. Tanaka, Y. Kubo, Y. Yokoyama, A. Toda, K. Taguchi, H. Kajioka, Kinetics of phase separation and coarsening in dilute surfactant pentaethylene glycol monododecyl ether solutions, J. Chem. Phys. 135 (2011) 234503.

[34] V.M. Kendon, M.E. Cates, I. Pagonabarraga, J.C. Desplat, P. Blandon, Inertial effects in three-dimensional spinodal decomposition of a symmetric binary fluid mixture: a lattice Boltzmann study, J. Fluid Mech. 440 (2001) 147–203.

[35] S. Puri, B. Dünweg, Temporally linear domain growth in the segregation of binary fluids, Phys. Rev. A 45 (1992) R6977–R6980.

[36] C. Datt, S.P. Thampi, R. Govindarajan, Morphological evolution of domains in spinodal decomposition, Phys. Rev. E 91 (2015) 010101(R).

[37] M. Laradji, S. Toxvaerd, O.G. Mountain, Molecular dynamics simulation of spinodal decomposition in three-dimensional binary fluids, Phys. Rev. Lett. 77 (1996) 2253–2256.

[38] A.K. Thakre, W.K. den Ohe, W.J. Briels, Domain formation and growth in spinodal decomposition in a binary fluid by molecular dynamics simulations, Phys. Rev. E 77 (2008) 011503.

[39] S. Ahmad, S.K. Das, S. Puri, Kinetics of phase separation in fluids: a molecular dynamics study, Phys. Rev. E 82 (2010) 040107.

[40] S. Ahmad, S.K. Das, S. Puri, Crossover in growth laws for phase separating binary fluids: molecular dynamics simulations, Phys. Rev. E 85 (2012) 031140.

[41] S. Ahmad, S. Puri, S.K. Das, Phase separation of fluids in porous media: a molecular dynamics study, Phys. Rev. E 90 (2014) 040302(R).

[42] S.K. Das, S. Roy, S. Majumder, S. Ahmad, Finite-size effects in dynamics: critical versus coarsening phenomena, Phys. Rev. E 97 (2012) 66006.

[43] H. Kabrede, R. Hentschke, Spinodal decomposition in a 3D Lennard-Jones system, Physica A 361 (2006) 485–493.

[44] S. Majumder, S.K. Das, Universality in fluid domain coarsening: the case of vapor–liquid transition, Europhys. Lett. 95 (2012) 46002.

[45] S. Roy, S.K. Das, Nucleation and growth of droplets in vapor–liquid transitions, Phys. Rev. E 85 (2012) 050602.

[46] S. Roy, S.K. Das, Dynamics and growth of droplets close to the coexistence curve in fluids, Soft Matter 9 (2013) 4178–4187.

[47] S. Roy, S.K. Das, Effects of domain morphology on kinetics of fluid phase separation, J. Chem. Phys. 139 (2013) 044911.

[48] S.W. Koch, R.C. Desai, F.F. Abraham, Dynamics of phase separation in two-dimensional fluids: spinodal decomposition, Phys. Rev. A 27 (1983) 2152–2167.

[49] J. Midya, S.K. Das, in preparation.

[50] D.S. Fisher, D.A. Huse, Nonequilibrium dynamics of spin glass, Phys. Rev. B 38 (1988) 373–385.

[51] S.N. Majumdar, A.J. Bray, S.J. Cornell, C. Sire, Global persistence exponent for nonequilibrium critical dynamics, Phys. Rev. Lett. 77 (1996) 3704–3707.

[52] J.-P. Hansen, I.R. McDonald, Theory of Simple Liquids, Academic Press, London, 2008.

[53] D.P. Landau, K. Binder, A Guide to Monte Carlo Simulations in Statistical Physics, Cambridge University Press, 2009.

[54] I. Schmidt, K. Binder, Dynamics of wetting transitions: a time-dependent Ginzburg–Landau treatment, Z. Phys. B, Condens. Matter 67 (1987) 369.

[55] S.K. Das, J. Horbach, K. Binder, Kinetics of phase separation in thin films: lattice versus continuum models for solid binary mixtures, Phys. Rev. E 79 (2009) 021602.

[56] P.C. Hohenberg, B.I. Halperin, Theory of dynamic critical phenomena, Rev. Mod. Phys. 49 (1977) 436–479.

[57] K. Kaski, K. Binder, J.D. Gunton, A study of cell distribution functions of the three dimensional Ising model, Phys. Rev. B 29 (1984) 3996–4009.

[58] S. Ramaswamy, The mechanics and statistics of active matter, Annu. Rev. Condens. Matter Phys. 1 (2010) 323–345.

[59] M.P. Allen, D.J. Tildesley, Computer Simulations of Liquid, Clarendon, Oxford, 1987.

[60] D. Frenkel, B. Smit, Understanding Molecular Simulation: From Algorithms to Applications, Academic Press, San Diego, 2002.

[61] D.C. Rapaport, The Art of Molecular Dynamics Simulations, Cambridge University Press, 2004.

[62] P. Nikuman, M. Karttunen, I. Vattulainen, How would you integrate the equations of motion in dissipative particle dynamics simulations?, Comput. Phys. Commun. 153 (2003) 407–423.

[63] S.D. Stoyanov, R.D. Groot, From molecular dynamics to hydrodynamics: a novel Galilean invariant thermostat, J. Chem. Phys. 122 (2005) 114112.

[64] C. Pastorino, T. Kreer, M. Müller, K. Binder, Comparison of dissipative particle dynamics and Langevin thermostats for out-of-equilibrium simulations of polymeric systems, Phys. Rev. E 76 (2007) 026706.

[65] A. Winkler, P. Virnau, K. Binder, R.G. Winkler, G. Gompper, Hydrodynamic mechanisms of spinodal decomposition in confined colloid–polymer mixtures: a multiparticle collision dynamics study, J. Chem. Phys. 138 (2013) 0544901.

[66] E.A. Koopman, C.P. Lowe, Advantages of a Lowe–Andersen thermostat in molecular dynamics simulations, J. Chem. Phys. 124 (2006) 204103.

[67] S. Roy, S.K. Das, Finite-size scaling study of shear viscosity anomaly at liquid–liquid criticality, J. Chem. Phys. 141 (2014) 234502.

[68] J.V. Sengers, R.A. Perkins, Fluids near critical points, in: M.J. Assael, A.R.H. Goodwin, V. Vesovic, W.A. Wakehan (Eds.), Transport Properties of Fluids: Advances in Transport Properties, IUPAC, RSC publishing, Cambridge, 2014, pp. 337–361.

[69] A. Chen, E.H. Chimowitz, S. De, Y. Shapir, Universal dynamic exponent at the gas liquid transition from molecular dynamics, Phys. Rev. Lett. 95 (2005) 255701.

[70] S. Roy, S.K. Das, Transport phenomena in fluids: finite-size scaling for critical behavior, Europhys. Lett. 94 (2011) 36001.

[71] R.F. Berg, M.R. Moldover, G.A. Zimmerli, Viscoelasticity of Xenon near the critical point, Phys. Rev. Lett. 82 (1999) 920–923.

[72] H.C. Burstyn, J.V. Sengers, Decay rate of critical concentration fluctuation in a binary liquid, Phys. Rev. A 25 (1982) 448–465.

[73] J.K. Bhattacharjee, I. Iwanowski, U. Kaatze, Bulk viscosity universality and scaling function near the binary liquid consolute point, J. Chem. Phys. 131 (2009) 174502.

[74] J.K. Bhattacharjee, U. Kaatze, S.Z. Mirzaev, Sound attenuation near the demixing point of binary liquids: interplay of critical dynamics and noncritical kinetics, Rep. Prog. Phys. 73 (2010) 066601.

[75] A.Z. Panagiotopoulos, Direct determination of phase coexistence properties of fluids by Monte Carlo simulation in a new ensemble, Mol. Phys. 61 (1987) 813–826.

[76] M.E. Fisher, M.N. Barber, Scaling theory for finite-size effects in the critical region, Phys. Rev. Lett. 28 (1972) 1516–1519.

[77] S. Ahmad, F. Corberi, S.K. Das, E. Lippiello, S. Puri, M. Zannetti, Aging and crossover in phase separating fluid mixtures, Phys. Rev. E 86 (2012) 061129.

[78] S. Majumder, S.K. Das, Effects of density conservation and hydrodynamics on aging in nonequilibrium processes, Phys. Rev. Lett. 111 (2013) 055503.

[79] R.A.L. Jones, Laura J. Norton, Edward J. Kramer, Frank S. Bates, Pierre Wiltzius, Surface-directed spinodal decomposition, Phys. Rev. Lett. 66 (1991) 1326–1329.

[80] S. Puri, K. Binder, Surface-directed spinodal decomposition: phenomenology and numerical results, Phys. Rev. A 46 (1992) R4487–R4489.

[81] H. Tanaka, Interplay between wetting and phase separation in binary fluid mixtures: roles of hydrodynamics, J. Phys. Condens. Matter 13 (2001) 4637–4674.

[82] S. Bastea, S. Puri, J.L. Lebowitz, Surface-directed spinodal decomposition in binary fluid mixtures, Phys. Rev. E 63 (2001) 041513.

[83] S.K. Das, S. Puri, J. Horbach, K. Binder, Spinodal decomposition in thin films: molecular-dynamics simulations of a binary Lennard-Jones fluid mixture, Phys. Rev. E 73 (2001) 031604.

[84] S.K. Das, S. Puri, J. Horbach, K. Binder, Molecular dynamics study of phase separation kinetics in thin films, Phys. Rev. Lett. 96 (2006) 016107.
[85] M.J.A. Hore, M. Laradji, Dissipative particle dynamics simulation of the interplay between spinodal decomposition and wetting in thin film binary fluids, J. Chem. Phys. 132 (2010) 024908.
[86] K. Binder, S. Puri, S.K. Das, J. Horbach, Phase separation in confined geometries, J. Stat. Phys. 138 (2010) 51–84.
[87] P.K. Jaiswal, K. Binder, S. Puri, Phase separation of binary mixtures in thin films: effects of an initial concentration gradient across the film, Phys. Rev. E 85 (2012) 041602.
[88] P.K. Jaiswal, S. Puri, S.K. Das, Hydrodynamic crossovers in surface-directed spinodal decomposition and surface enrichment, Europhys. Lett. 97 (2012) 16005.
[89] E.A.G. Jamie, R.P.A. Dullens, D.G.A.L. Aarts, Spinodal decomposition of a confined colloid–polymer system, J. Chem. Phys. 137 (2012) 204902.
[90] S.J. Mitchell, D.P. Landau, Phase separation in a compressible 2D Ising model, Phys. Rev. Lett. 97 (2006) 025701.